Open Ceramics 7 (2021) 100145

Contents lists available at ScienceDirect

Open Ceramics

journal homepage: www.editorialmanager.com/oceram

AlF_3-assisted flux growth of mullite whiskers and their application in fabrication of porous mullite-alumina monoliths

Amanmyrat Abdullayev [a], Detlef Klimm [b], Franz Kamutzki [a], Aleksander Gurlo [a], Maged F. Bekheet [a,*]

[a] Fachgebiet Keramische Werkstoffe, Advanced Ceramic Materials, Institute of Materials Science and Technology, Technische Universität Berlin, 10623, Berlin, Germany
[b] Leibniz-Institut für Kristallzüchtung, Max-Born-Str. 2, 12489, Berlin, Germany

ARTICLE INFO

Keywords:
Mullite
Molten salt
Crystal growth
Freeze casting
Reinforced ceramics

ABSTRACT

Mullite is a promising material with its competitive thermochemical and mechanical properties. Although mullite could be obtained by several synthesis methods, the flux method emerges with its advantages over other methods. However, obtaining mullite whiskers with a high aspect ratio and length for ceramic reinforcements is still challenging. In this work, mullite whiskers were grown from AlF_3-assisted flux. The addition of AlF_3 to flux salt not only decreases the formation temperature of mullite to as low as 700 °C and suppresses the formation of corundum side phase, but also increases the length and aspect ratio of the whiskers. The obtained mullite whiskers were used as reinforcement for porous alumina monoliths prepared by the freeze casting route and subsequent sintering at 1500 °C. The fabricated mullite-alumina monoliths show competitive compressive strength of 25.7 MPa while having as high as 70.6% porosity, which makes them a potential candidate for membrane applications.

1. Introduction

Mullite is an aluminosilicate ceramic with a composition ranging from $3Al_2O_3{\cdot}2SiO_2$ (3:2 mullite) to $2Al_2O_3{\cdot}SiO_2$ (2:1 mullite). Mullite whiskers have been applied for the reinforcement of ceramics and metals as well as catalytic and membrane supports [1,2]. Typically, the whiskers are synthesized from the corresponding oxides above 1200 °C by a solid-state method. Such high synthesis temperatures are required due to the slow diffusion of the reactants; however, they limit the practical usage of mullite whiskers [3]. Thus, the flux method has recently emerged as an alternative method to obtain mullite whiskers [4–6]. The advantage of the flux method is the reduction in synthesis temperature (below 1200 °C) due to the faster transport of reactants in a liquid (molten salt) phase [7]. Moreover, when salts melt, they form a pool of ionized cations and anions, and a strong polarising force enables the breakdown of strong bonds of reactants such as those found in alumina and silica compounds [8]. Another advantage of the flux method is that mullite whiskers are produced directly in powder form in contrast to other methods that first produce the rigid solid body of mullite before the crushing or grinding into powder form for further applications.

In the numerous works on the flux synthesis of mullite whiskers [4,5,9–15], the influence of various salts [5,9,12], alumina [4,5] and silica sources [10,11], synthesis time/temperature [13], and various additives [14,15] on mullite formation temperature and mullite whisker morphology have been intensively investigated. Usually, Na_2SO_4 has been used as a flux salt when $Al_2(SO_4)_3$ and amorphous SiO_2 are used as reactants materials. Yet, temperatures of around 900 °C are required to obtain highly crystalline mullite using this flux method.

Fluorine-containing compounds, mainly AlF_3, have recently been applied to synthesize crystalline mullite whiskers at lower temperatures (~900 °C) with an intermediate formation of highly reactive gaseous species, i.e., solid-gas reaction routes [16,17]. AlF_3 provides aluminium cations for mullite formation and fluorine ions that can catalyze the crystallization of mullite. Nucleophilic fluoride ions can accelerate the dissolution of alumina or silica [8]. Thus, adding a small amount of AlF_3 to the flux salt could facilitate the formation of mullite whiskers as well as reduce the flux viscosity [18,19]. This, in turn, reduces the constraints for mullite growth and leads to the formation of whiskers with a high aspect ratio.

Due to its superior thermomechanical and chemical properties, mullite is considered a promising material for reinforcing ceramic, metallic, and composite materials [20]. Most previous studies focused on

* Corresponding author.
E-mail address: maged.bekheet@ceramics.tu-berlin.de (M.F. Bekheet).

https://doi.org/10.1016/j.oceram.2021.100145
Received 26 April 2021; Received in revised form 4 June 2021; Accepted 16 June 2021
Available online 18 June 2021

Table 1
The chemical composition of the rice husk derived amorphous silica determined by XRF (the elements are expressed as their most abundant oxide).

Oxides	SiO_2	Al_2O_3	Fe_2O_3	MnO	MgO	CaO	Na_2O	K_2O	TiO_2	P_2O_5	L.O·I
wt%	94.34	<0.2	<0.5	0.01	0.07	<0.3	<0.12	<0.1	0.05	0.2	4.11

Table 2
Specimens studied in this work.

Sample	Synthesis temperature, °C	The molar ratio of components			
		$Al_2(SO_4)_3{\cdot}3H_2O$	Na_2SO_4	$AlF_3{\cdot}3H_2O$	SiO_2
M0-10	1000	1.0	4.6	–	0.67
M5-10				0.11	0.70
M10–10				0.22	0.74
M20–10				0.5	0.83
M0-11	1100			–	0.67
M20–11				0.5	0.83
M0-9	900			–	0.67
M20–9				0.5	0.83
M0-8	800			–	0.67
M20–8				0.5	0.83
M0-7	700			–	0.67
M20–7				0.5	0.83

using either in-situ formed mullite whiskers or continuous mullite fibers [21–24]. The influence of ex-situ synthesized mullite whiskers on the mechanical properties of composite materials was addressed in a few works [25,26]. These works revealed that the addition of mullite whiskers increased the tensile and flexural strength of alumina matrices. It was concluded that the ex-situ formed mullite whiskers, particularly those with a high aspect ratio, can be used for reinforcing different materials such as porous ceramics for insulation, filtration, and catalysis applications.

Accordingly, in this study, highly crystalline mullite whiskers are grown using the fluoride-assisted flux method and the role of AlF_3 in the mullite synthesis as well as its influence on the properties of the grown mullite whiskers are evaluated. The as-grown mullite whiskers with high aspect ratios are used to reinforce freeze-cast porous alumina monolith, and their influence on the mechanical stability of the obtained porous ceramic bodies is also investigated.

2. Materials and methods

2.1. Materials

$Al_2(SO_4)_3{\cdot}18H_2O$ (≥97%, Merck, Germany), Na_2SO_4 (99%, Merck, Germany), $AlF_3{\cdot}3H_2O$ (≥97%, Ventron, Germany), and amorphous SiO_2 from waste rice husk were used for whisker synthesis. Tert-butanol (TBA, 99%, Merck, Germany), citric acid (99%, Carl Roth, Germany), polyvinyl butaryl (PVB, ≥97%, Kuraray, Japan) and high purity alumina (AKP-50, 99.99%, Sumitomo, Japan) were used for monolith fabrication by freeze casting. Amorphous silica is obtained from waste rice husk using the method reported elsewhere [27,28]. Briefly, waste rice husk is first leached with a citric acid solution at 50 °C for 4 h by stirring to remove impurities such as Na, K, etc. Then, the leached samples are washed three times with excess water and dried at 100 °C overnight. They are subsequently calcined at 600 °C for 6 h. The results of XRF and XRD characterizations confirmed the chemical composition of the materials with 94 wt% of amorphous SiO_2, see Table 1, where the rest is loss-on-ignition and a minor amount of other metal oxides. BET analysis reveals that the specific surface area of the obtained silica is about 234.1 m^2/g.

2.2. Synthesis of mullite whiskers

$Al_2(SO_4)_3{\cdot}18H_2O$ was first calcined at 300 °C for 12 h to obtain the more stable $Al_2(SO_4)_3{\cdot}3H_2O$, which allows us to weigh accurately the exact amount required to obtain the stoichiometric mullite. Moreover, this dehydration step is important to reduce the amount of water vapour formed by the decomposition of $Al_2(SO_4)_3{\cdot}18H_2O$ during the synthesis, which results in the degradation of the formed crystalline mullite at high temperatures [26]. For all experiments, Na_2SO_4:$Al_2(SO_4)_3{\cdot}3H_2O$ molar ratio was fixed at 4.6:1.0 to achieve a low melting point of the flux salt of about 650–700 °C [6]. Various amounts of $AlF_3{\cdot}3H_2O$ (corresponding to 5, 10, and 20 mol% of total aluminium atoms in the powder mixture) were added to obtain the samples M5, M10, and M20, respectively. For comparison, the reference sample M0 was also prepared without any addition of $AlF_3{\cdot}3H_2O$. The amount of silica was adjusted for each batch to maintain a 3:2 mullite stoichiometry considering the total aluminium amount in the powder mixtures, as shown in Table 2. The obtained powder mixtures were manually ground in mortar and pestle for 15 min. The mullite whiskers were grown by heating the ~11 g of powder mixtures in an alumina crucible (height of 40 mm and diameter of 20 mm) covered with a lid to minimize the evaporation of salts. The samples were heated to target temperatures (700–1000 °C, see Table 2) with a heating rate of 5 °C/min and a dwell time of 3 h. The grown mullite whiskers were separated from the flux residue by dissolving salts in hot water under ultrasonication, followed by washing with boiling water three times. The obtained white powders were finally filtered off and dried overnight at 100 °C in an ambient atmosphere. The final samples are named according to the synthesis temperature, e.g., specimens obtained from M0 at 700 °C and 1100 °C are named as M0-7 and M0-11, respectively.

2.3. Fabrication of porous monolith

Among all samples, mullite whiskers grew from the powder mixture containing 20 mol. % of AlF_3 at 1000 °C (M20-10) possess the highest aspect ratio of 37.86 ± 11.73. Therefore, the sample M20-10 was chosen for the fabrication of mullite-alumina porous monoliths, as described below. Several mullite alumina (MA) powder mixtures were prepared by mixing alumina powder with the mullite whiskers in the weight ratio of 100:0 (MA0), 95:5 (MA5), 90:10 (MA10) and 80:20 (MA20). 15 g of the MA powder mixture was then added into 15 g of hot premixed TBA solution at 50 °C. The premixed TBA solution contains 2 wt% citric acid as a dispersant and 1 wt% PVB as a binder. This slurry was stirred for 30 min while maintaining the temperature at 50 °C. The obtained slurry was poured into an acrylic glass mold and cooled with a 2 °C/min rate until it has frozen completely. Details about the freeze casting setup are presented elsewhere [29]. The solidified cylindrical samples (with a diameter of 10 mm and a height of 25 mm) were dried in a freeze dryer (VaCo 5, Zirbus, Germany) under a vacuum (−60 °C and 0.1 mbar). Dried samples were sintered at 1500 °C with a 5 °C/min heating rate and 2 h of dwell time.

2.4. Characterization of mullite whiskers

The crystallinity and phase compositions of the samples were analyzed by X-ray powder diffraction technique in a D8 Advance (Bruker, Germany) using CoK_α radiation in the 2θ range of 10–90° with a step size of 0.02° and step time of 8 s. Rietveld refinement of the powder XRD data was performed using the FullProf suite [30]. The profile function of Thompson−Cox Hastings pseudo-Voigt convoluted with axial divergence asymmetry was used in all refinements [31]. The resolution function of the diffractometers was obtained from the structure refinement of a LaB_6 standard. The microstructure of synthesized powders was analyzed with a scanning electron microscopy (SEM) (LEO 1530, Zeiss, Germany), where a small amount of powder was stuck to the adhesive carbon tape

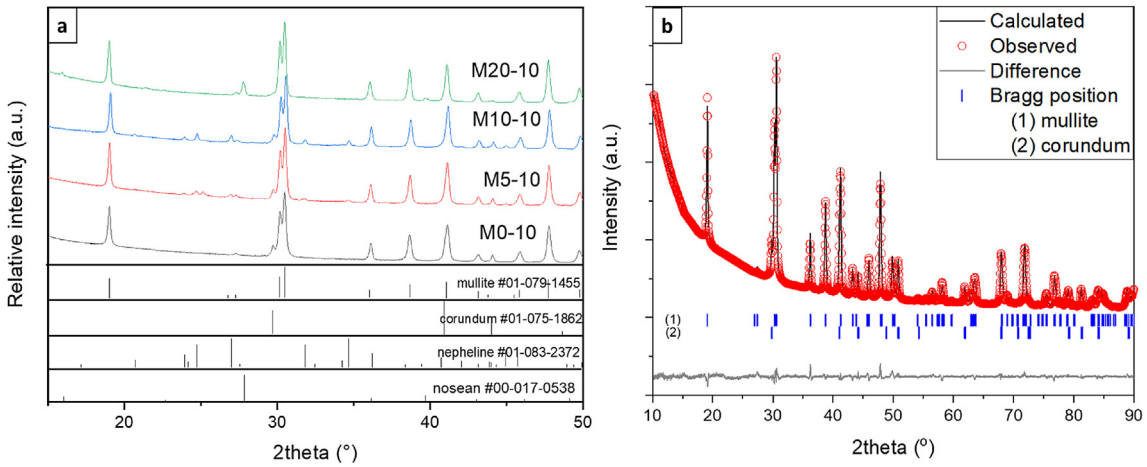

Fig. 1. a) XRD patterns of mullite whiskers synthesized at 1000 °C without $AlF_3{\cdot}3H_2O$ (M0-10) and with 5 (M5-10), 10 (M10-10) and 20 (M20-10) mol% of $AlF_3{\cdot}3H_2O$. b) Structure refinement of X-ray powder diffraction data collected at room temperature using the orthorhombic structure of mullite (i.e., SG: *Pbam*) showing the observed (red circle), calculated (black solid line) and difference (gray solid line) intensities, as well as the calculated Bragg reflections (blue tick marks). (For interpretation of the references to colour in this figure legend, the reader is referred to the Web version of this article.)

Table 3
Composition (wt.%) of crystalline phases in the synthesized powders from the Rietveld analysis of the XRD data; standard deviations are shown in parentheses.

Sample	Mullite	Corundum	**Nepheline ($Na_4Al_4Si_4O_{16}$)**	Nosean ($Na_8Al_6Si_6O_{24}(SO_4)$	Mullite and alumina weight fraction (%) without considering nepheline or nosean	
					Mullite	Corundum
M0-10	87.0 (0.68)	13.0 (0.25)	–	–	87.0	13.0
M5-10	85.8 (0.53)	11.3 (0.12)	2.9 (0.15)	–	88.4	11.6
M10–10	82.7 (0.49)	11.7 (0.13)	5.6 (0.12)	–	87.7	12.3
M20–10	92.4 (0.64)	3.0 (0.13)	–	4.6 (0.12)	96.9	3.1

and then sputtered with gold layer. The average dimension of mullite whiskers was determined from SEM images using image analysis software ImageJ [32]. At least ten randomly selected particles were studied to get the average length and aspect ratio of the mullite whiskers. The formation of mullite whiskers from the precursor powder mixture was investigated by thermogravimetric (TG) and differential thermal analysis (DTA) using the STA 449F3 (Netzsch, Germany). The powder mixtures were heated in an alumina crucible up to 1200 °C at a heating rate of 10 °C/min under an atmosphere of oxygen and argon (20 vol% O_2 – 80 vol% Ar). For some samples, effluent gases from TG-DTA were analyzed using a mass spectroscopy (MS) devise (GSD-320 O1, Pfeiffer Vacuum, Germany).

2.5. Characterization of MA monoliths

Shrinkage of MA monoliths was determined by measuring the diameter of monoliths before and after sintering. The porosity of samples was measured by the Archimedes method using water according to the ASTM C-373-18 standard [33]. The percentage of open porosities in the MA monoliths was calculated according to Eq. (1):

$$\left(P = 100 * \left[\left(W_{sat} - W_{dry}\right) / \left(W_{sat} - W_{im}\right)\right],\right. \quad (1)$$

where P is the percentage of open porosities and W_{dry}, W_{sat}, and W_{im} are the weights of dry, saturated, and immersed (in water) monoliths, respectively. Pore size distribution was analyzed with a mercury intrusion porosimeter (MIP) (2000 WS, Carlo Erba, Italy).

The microstructure of monoliths was investigated via SEM (LEO 1530, Zeiss, Germany). The specimens for SEM characterization were cut from the prepared monolith using a diamond disc and then sputtered with a gold layer. Measurement of the compressive strength of monoliths with ~10 mm diameter and 15 mm height were performed with a RetroLine testing machine (Z005, Zwick Roell, Germany), where at least 3 replicas from each sample were tested and the average values obtained.

3. Results and discussion

3.1. Effect of AlF_3 on the mullite formation

3.1.1. Effect of AlF_3 content on the phase composition

As shown in Fig. 1 a, b and Table 3, the mullite whiskers grown from AlF_3-free precursor at 1000 °C contains 13 wt% of corundum (α-Al_2O_3) as an impurity in addition to the mullite phase. The formation of corundum at these experimental conditions is consistent with previous works, which reported that both corundum and mullite phases are

Table 4
Rietveld refinement results with cell parameters, crystallite size and calculated molar content of Al_2O_3 of mullite.

	Cell parameters of mullite			**Crystallite size, Å**	**Max. strain, $*10^{-3}$**	**R_{wp}**	**X^2**	**Al_2O_3 content of mullite, mol%**
	a	b	c					
M0-10	7.56688 (0.00019)	7.69614 (0.00016)	2.88106 (0.00006)	525.2 (0.53)	1.46 (0.0156)	3.42	4.60	63.8
M5-10	7.56552 (0.00019)	7.69801 (0.00016)	2.88332 (0.00006)	624.6 (0.40)	1.52 (0.0151)	3.10	4.94	63.6
M10-10	7.56770 (0.00019)	7.69914 (0.00016)	2.88440 (0.00006)	669.8 (0.64)	1.53 (0.0103)	3.23	4.82	63.9
M20-10	7.56575 (0.00024)	7.69597 (0.00020)	2.88439 (0.00007)	726.2 (0.50)	1.64 (0.0096)	3.39	6.39	63.7

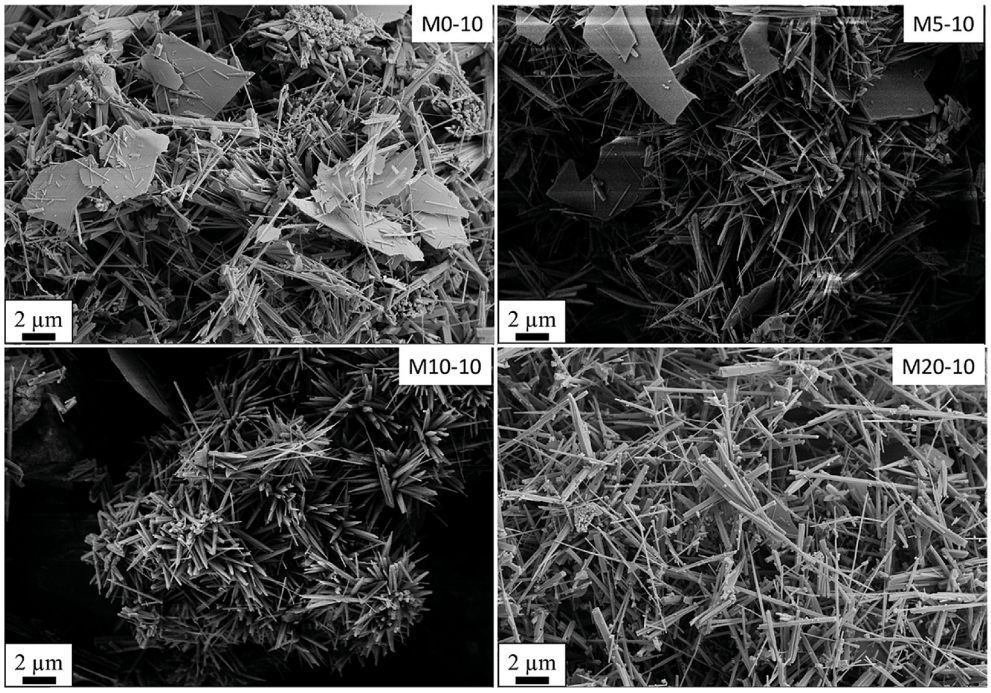

Fig. 2. The microstructure of mullite whiskers synthesized at 1000 °C without $AlF_3{\cdot}3H_2O$ (M0-10) and with 5 (M5-10), 10 (M10-10) and 20 (M20-10) mol% of $AlF_3{\cdot}3H_2O$.

thermodynamically stable in the salt flux at the synthesis conditions [5]. However, using an excessive amount of silica could facilitate the formation of the mullite phase and suppress the transformation of the reactive alumina phase into corundum [5,9,10]. No remarkable change in the amount of corundum phase was observed in the M5-10 and M10-10 samples when a small amount of AlF_3 was applied during the synthesis. For example, samples M5-10 and M10-10 contain around 12 wt% of corundum as a side phase, without taking into account nepheline ($Na_4Al_4Si_4O_{16}$). In contrast, the amount of corundum was significantly decreased to ~3 wt% when a higher amount of AlF_3 was used (i.e., in the M20-10 sample). From these results, it can be concluded that the mullite formation reaction can also be facilitated with the aid of AlF_3 while suppressing corundum formation.

Crystallite sizes and cell parameters of mullite whiskers are determined from Rietveld refinement of XRD data and are presented in Table 4. With increasing AlF_3 content in the precursors, the crystallite size of mullite whiskers also increases from 52.5 nm to 72.6 nm, which is due to the decrease in the viscosity of salt flux. This decrease in flux viscosity leads to lesser constraints for crystal growth, resulting in larger crystallites [14,15].

Mullite has an orthorhombic crystal structure with stoichiometries ranging from relatively silica-rich $3Al_2O_3{\cdot}2SiO_2$ (3:2 mullite) to alumina-rich $2Al_2O_3{\cdot}SiO_2$ (2:1 mullite). The length of the *a*-axis has a linear relationship with the molar content of Al_2O_3 in mullite, i.e., the chemical composition of mullite can be estimated using the equation proposed by Ban and Okada [34]:

$$Al_2O_3\ (\text{mol. \%}) = 1443\ (\text{length of } an \text{ axis in nm}) - 1028.06 \quad (2)$$

The mullite whiskers obtained in this work have around 64 mol% Al_2O_3 (see Table 4) which corresponds to an Al_2O_3:SiO_2 ratio of 1.8. These results suggest that the obtained mullite has a chemical composition between 3:2 and 2:1 mullites. This region is known as the stability region of mullite and is considered a technically promising composition [35]. Moreover, these results indicate that the molar content of Al_2O_3 in the obtained mullites is independent of the AlF_3 amount.

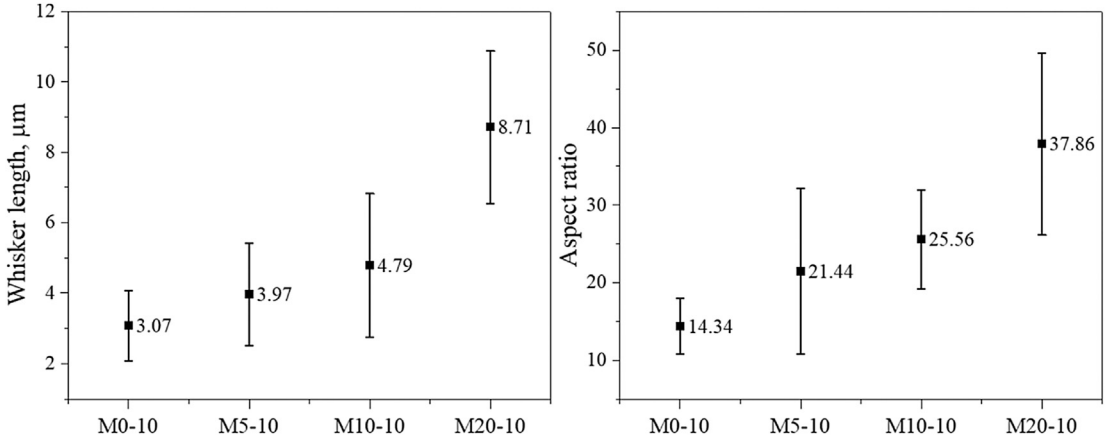

Fig. 3. Length and aspect ratio of mullite whiskers obtained at 1000 °C as a function of AlF_3 content. With increasing AlF_3 content, the length and aspect ratio of mullite whiskers increased.

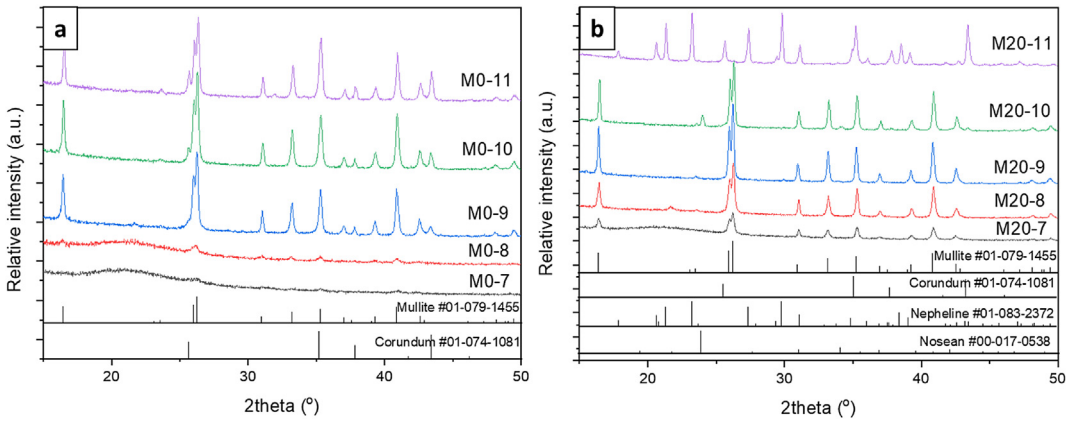

Fig. 4. XRD pattern of the samples obtained from a) AlF_3-free M0 powder mixture and b) M20 powders containing 20 mol% AlF_3 at synthesis temperatures of 700 °C (M0-7 and M20-7), 800 °C (M0-8 and M20-8), 900 °C (M0-9 and M20-9), 1000 °C (M0-10 and M20-10) and 1100 °C (M0-11 and M20-11).

3.1.2. *Effect of AlF_3 content on the microstructure*

Fig. 2 shows SEM images of mullite samples synthesized at 1000 °C using different amounts of AlF_3. The morphology of the samples is changed from platelet-like to needle-like particles with increasing the amount of AlF_3 in the precursors. This finding is consistent with the previous works that report the needle-like microstructure of mullite synthesized by the flux method [9]. Platelet-like particles can be attributed to the unreacted alumina, which agrees with previous work that showed the formation of similar alumina platelets in the Na_2SO_4–$Al_2(SO_4)_3$ flux [6]. The small amount of glassy-like particles observed in some samples might be related to unreacted amorphous silica [5,17].

As depicted in Fig. 3, the length and aspect ratio of mullite whiskers also increase with increasing AlF_3 amount in the starting precursors. M0-10 contains mullite whiskers with an average length and aspect ratio of 3.07 ± 1.00 μm and 14.34 ± 3.59, respectively, while sample M20-10 exhibited an average mullite whisker length and aspect ratio of 8.71 ± 2.17 μm and 37.86 ± 11.73, respectively. The greater aspect ratio of the whisker means more excellent mechanical stability [36]. The length of mullite whiskers depends on flux viscosity, whereas their growth in the *c* direction is facilitated in the low viscous flux system. Here AlF_3 has led to the formation of flux with low viscosity. Consequently, fewer constraints exist to hinder the growth of anisotropic whiskers [15].

The size of whiskers is crucial because fine whiskers are challenging to handle, causing high health risks. Thus, the synthesis of mullite with a longer length and high aspect ratio would not only be advantageous for reinforcing, but also enable easier handling [37].

3.1.3. *Effect of AlF_3 on the formation temperature of mullite*

Fig. 4 a and b show the XRD patterns of the specimens obtained from M0 and M20 samples at different temperatures, respectively. As shown in Fig. 4a, only small amounts of nanocrystalline mullite are formed in M0-7 and M0-8 samples upon the heating of AlF_3-free precursor M0 at 700 °C and 800 °C, respectively. Highly crystalline mullite whiskers were formed in the M0-9, M0-10, and M0-11 by increasing the synthesis temperatures above 900 °C. This finding agrees with the literature, where it is reported that although mullite starts to crystallize at 800 °C in the Na_2SO_4–$Al_2(SO_4)_3$ flux, temperatures higher than 900 °C are required to obtain highly crystalline mullite [38].

As displayed in Fig. 4b, the addition of 20 mol% of AlF_3 to the salt flux lowers the formation temperature of mullite to 700 °C, and highly crystalline mullite can be obtained at 800 °C. In contrast to M0, above 900 °C, nosean ($Na_8Al_6Si_6O_{24}(SO_4)$) and nepheline ($Na_4Al_4Si_4O_{16}$) are observed in M20–9 and M20-10 samples. Moreover, when the synthesis temperature of 1100 °C was applied, there was no mullite observed, but only corundum and nepheline phases. These results are consistent with previous works that reported the decompositions of mullite into corundum and sodium aluminosilicate at higher synthesis temperatures (e.g., 1200 °C [39] or 1400 °C [15]) even in the absence of AlF_3. However, these results show that the addition of AlF_3 leads to the decomposition of mullite even at lower temperatures, which can be attributed to the higher nucleophilicity of fluoride ions in the flux.

3.1.4. *Mechanism of mullite formation*

The mechanism of the formation of mullite whiskers in the presence of AlF_3 was followed by thermal analysis. Fig. 5 a, b and c show TG-DTA curves collected during heating of the powder mixtures of flux-forming salts only ($Al_2(SO_4)_3$ + Na_2SO_4) (referred as S0), M0 and M20, respectively. Both M0 and M20 precursors exhibit small weight losses (3.0 wt% in case of M0 and 3.6 wt% in case of M20) during heating up to 200 °C, accompanied by a broad endothermic peak that can be attributed mainly to the evaporation of moisture and dehydration of $AlF_3{\cdot}3H_2O$ [40]. For all samples, a sharp endothermic peak observed at temperature 250 °C

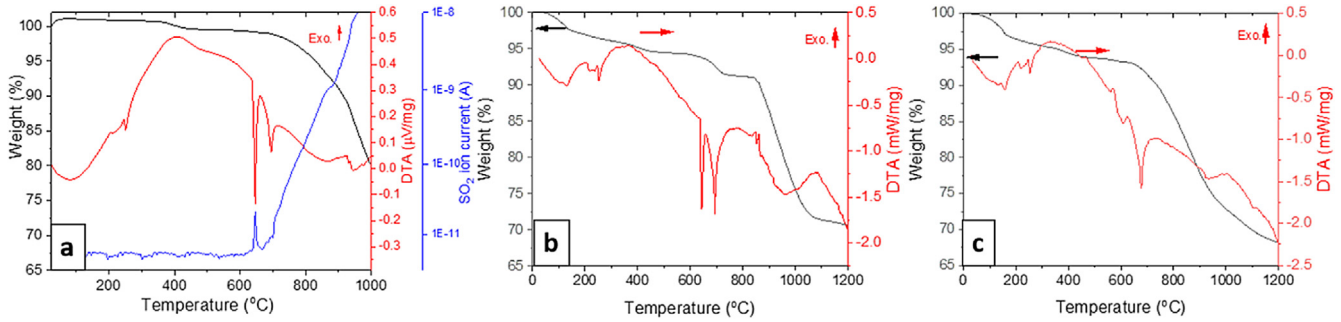

Fig. 5. (a) Simultaneous thermal analysis (STA) of flux-forming salts, i.e. $Al_2(SO_4)_3$ and Na_2SO_4: the evolution of SO_2 gas is observed by in situ mass spectrometry (blue solid line). (b–c) TG-DTA analysis during the formation of mullite whiskers from (b) AlF_3-free powder mixture (M0) and b) powder mixture containing 20 mol% AlF_3 (M20). (For interpretation of the references to colour in this figure legend, the reader is referred to the Web version of this article.)

associated with negligible weight loss can be assigned to the transitions of α-Na_2SO_4 into β-Na_2SO_4 phase [41]. With further increase in the temperature up to 600 °C, slight weight loss can be seen for all precursors related to the slow evolution of chemically-bonded water in $Al_2(SO_4)_3{\cdot}3H_2O$ salt [42].

For S0 and M0, two sharp endothermic peaks were observed at about 645 °C and 695 °C. The former one, accompanied by 2.2 wt% weight loss, is due to the decomposition of a small amount of $Al_2(SO_4)_3$ before flux formation, as illustrated in Eq. (3). This result is also confirmed by mass spectrometric analysis of effluent gases from S0 during TG-DTA, where a sharp peak of SO_2 ion current can be seen at 645 °C, see Fig. 5 a. The latter endothermic peak at 695 °C can be attributed to the melting process of the Na_2SO_4–$Al_2(SO_4)_3$ mixture (as in Eq. (4)) [6,43]. The sharp weight loss above 840 °C can be attributed to the evolution of SO_2 and O_2 from the system, indicating the formation of mullite as shown in Eq. (5).

$$Al_2(SO_4)_{3(s)} \overset{640\ ^\circ C}{\rightarrow} Al_2O_{3(s)} + 3SO_{2(g)} + 3/2O_{2(g)} \quad (3)$$

$$Al_2(SO_4)_{3(s)} + Na_2SO_{4(s)} \overset{690\ ^\circ C}{\rightarrow} flux\ \left(2Al^{+3} + 2Na^{+} + 4SO_4{}^{-2}\right) \quad (4)$$

$$6Al^{+3} + 9SO_4{}^{-2} + 2SiO_{2(s)} \overset{>850\ ^\circ C}{\rightarrow} mullite\left(3Al_2O_3 \cdot 2SiO_2\right)_{(s)} + 9SO_{2(g)} + 9/2O_{2(g)} \quad (5)$$

The endothermic peak at 695 °C, related to the flux formation in M0, was shifted to 675 °C when AlF_3 was added (i.e., in the case of M20), which might be due to the chemical reaction of AlF_3 with the molten salts, as proposed in Eq. (6). Moreover, in contrast to M0, the significant weight loss of precursor M20 starts at 650 °C instead of 840 °C. As explained above, the main weight-loss stage at this point is an indication of the mullite formation (see Eq. (5)). These results are confirmed by XRD results that reveal the formation of the mullite phase at 700 °C from precursor M20. The formation of mullite at a lower temperature in the presence of AlF_3 in the precursor can be explained by the formation of highly electronegative fluoride ions in the system, which facilitate the dissolution of strongly covalent O–Si–O bonds in SiO_2 (i.e. depolymerization of SiO_2 lattice), as described by Eqs. (7) and (8) [44,45].

$$Al_2(SO_4)_{3(s)} + Na_2SO_{4(s)} + AlF_{3(s)} \overset{675\ ^\circ C}{\rightarrow} flux\ \left(3Al^{3+} + 2Na^{+} + 4SO_4{}^{2-} + 3F^{-}\right) \quad (6)$$

$$SiO_{2(s)} + 2F^{-} \overset{700^\circ C}{\rightarrow} SiO_2F_2^{2-} \quad (7)$$

$$6Al^{3+} + 9SO_4{}^{2-} + 2SiO_2F_2^{2-} \overset{700\ ^\circ C}{\rightarrow} mullite\ \left(3Al_2O_3 \cdot 2SiO_2\right)_{(s)} + 9SO_{2(g)} + 9/2O_{2(g)} + 4F^{-} \quad (8)$$

The slight weight loss observed for the precursor M20 above 1000 °C can be attributed to the decomposition of mullite in molten Na_2SO_4, releasing gaseous SO_2 and O_2 according to Eq. (9) [15,46]:

$$mullite\left(3Al_2O_3 \cdot 2SiO_2\right)_{(s)} + 2Na_2SO_{4(l)} \overset{>1000^\circ C}{\rightarrow} nepheline\ \left(Na_4Al_4Si_4O_{16}\right)_{(s)} + Al_2O_{3(s)} + 2SO_{2(g)} + O_{2(s)} \quad (9)$$

This decomposition reaction is reported at 1200–1400 °C [15,39] without additives. However, our results showed that the presence of AlF_3 in the synthesis precursors could facilitate the decomposition even at lower temperatures. Hence, corundum and nepheline were observed instead of mullite in the sample synthesized at 1100 °C (i.e. in M20-11), as revealed by XRD analysis.

3.2. Effect of mullite whiskers on properties of porous alumina monolith

In the next step, we investigated the influence of the mullite whiskers on the properties of alumina monoliths prepared using freeze casting and subsequent sintering at 1500 °C. For this purpose, different weight ratios of M20-10 mullite whiskers which possess the highest aspect ratio were added during the processing of alumina monoliths. The shrinkage, compressive strength, porosity, pore size distribution and pore morphology of the obtained mullite-alumina (MA) monoliths were investigated. As presented in Table 5, the addition of 5 wt% mullite whisker sharply increased porosity from 65.8% to 75.6% and then porosity slowly decreased again with the further addition of mullite whisker. In contrast, the shrinkage of samples follows the opposite trend to that of porosity. In the absence of mullite whiskers, the diffusion and contact between alumina particles are high, resulting in well-sintered monoliths with high shrinkage and low porosity. In contrast, the presence of the mullite whiskers between the alumina particles hinders the densification process, increasing the porosity and lowering the shrinkage.

Table 5
Main properties of mullite whisker-alumina composites fabricated using TBA freeze casting method.

Sample	Porosity, %	Median pore diameter, μm	Compressive strength, MPa	Shrinkage, %
MA0	65.8	29	18.1	22.1
MA5	75.6	24	10.8	14.5
MA10	73.8	37	15.1	15.9
MA20	70.6	19	25.7	17.7

As shown in Table 5, the compressive strength of the obtained monoliths was also influenced by the addition of mullite whiskers. It is well-known that porosity and strength are inversely proportional to each other, i.e., when porosity increases, strength decreases [47]. Thus, monoliths MA5 and MA10 show lower compressive strength than monolith MA0. However, despite the fact that monolith MA20 has higher porosity (70.6%) than MA0 (65.8%), it still possesses higher compressive strength, 25.65 MPa vs 18.06 MPa. These results can be attributed to the bridging effect of whiskers, where they provided more contact points for particles. The high compressive strength and porosity of the monolith MA20 were quite competitive to the reported results in the literature [48,49]. The homogeneous pore structure and small pore size distribution of monolith MA20 can be another reason for its high mechanical strength. As shown in Fig. 6, the size of the pores was slightly decreased, and their distribution becomes more uniform by increasing mullite whisker content. Sample MA0 has bimodal pore size distribution, where the two modes are very close to each other. However, the addition of whiskers led to a clearly visible bimodal pore size distribution. These bimodal distributions can be explained as follows: i) the smaller pores are the interparticle pores and originated from the incomplete densification of particles (grain stacking); ii) larger pores are pores obtained by freezing of TBA or template of TBA crystals, which are consistent with previously reported results [50,51]. Based on these, when 5 wt% (MA5) or 10 wt% (MA10) of mullite whiskers were added, alumina particles and mullite whiskers are not very closely compacted, which is confirmed by their low shrinkages. A surprising observation was made with sample MA20, where it exhibited a monomodal pore size distribution. The interparticle pores which existed in other samples almost disappeared.

SEM characterization (Fig. 7) shows that all samples have a columnar structure, which is characteristic of TBA-based freeze casting [52]. These results indicate that the addition of mullite whiskers did not alter the general morphology of monoliths. However, the enhanced mechanical properties of monolith MA20 can be explained by the incorporation of mullite whiskers between alumina particles on the walls of pores, as can be seen from SEM images (Fig. 8). These mullite whiskers produce more bridges between alumina particles, preventing crack propagation in the walls. Thus, the monolith MA20 possesses the highest compressive strength even though it contains the highest porosity.

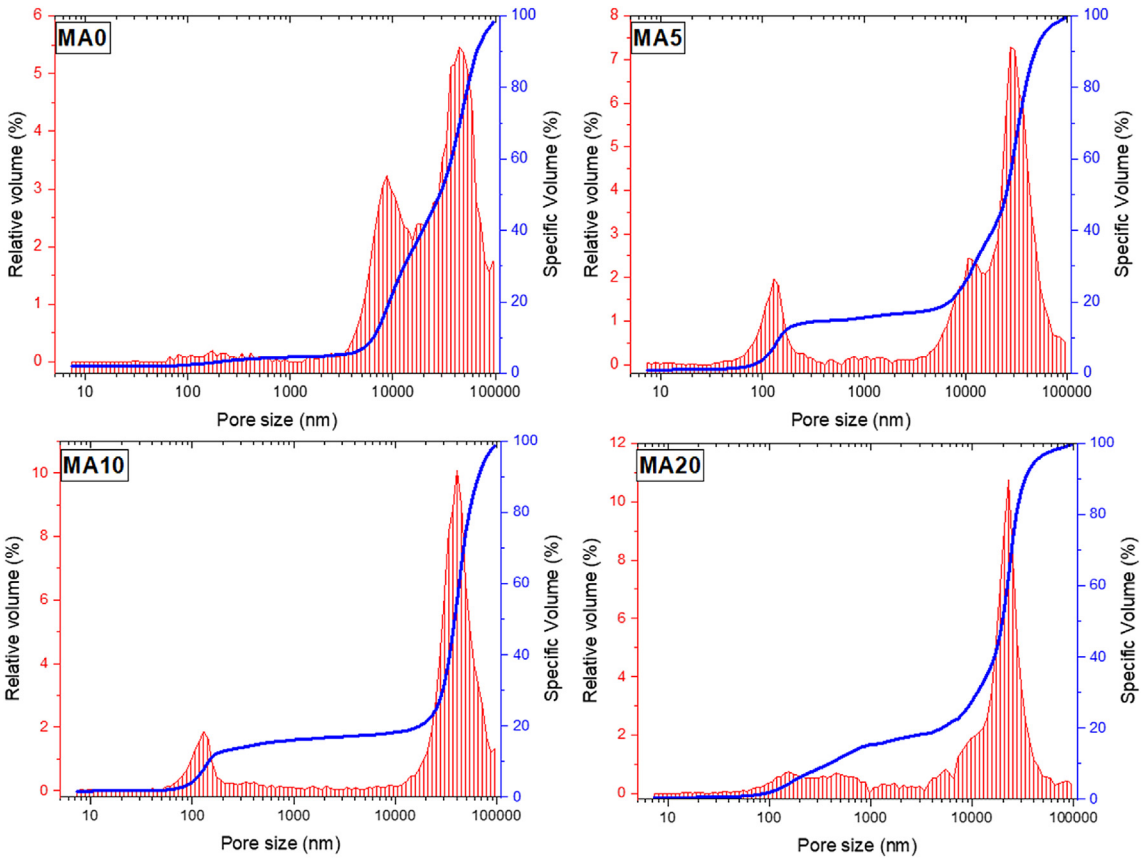

Fig. 6. The pore size distribution of mullite whisker-alumina monoliths prepared by freeze-casting TBA solution contains alumina/mullite whiskers with a weight ratio of 100:0 (MA0), 95:5 (MA5), 90:10 (MA10) and 80:20 (MA20).

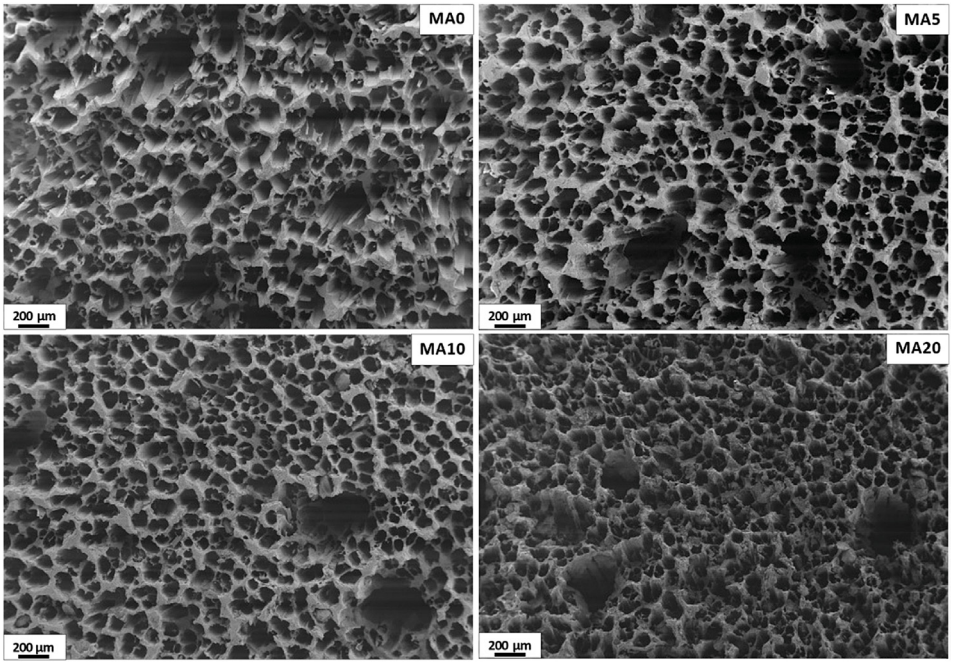

Fig. 7. SEM images of mullite whisker-alumina monoliths prepared by freeze-casting TBA solution contains alumina/mullite whiskers with the weight ratio of 100:0 (MA0), 95:5 (MA5), 90:10 (MA10) and 80:20 (MA20).

4. Conclusion

In this work, we have investigated the effect of AlF_3 addition on the compositional and microstructural properties of mullite whiskers that grew in Na_2SO_4–$Al_2(SO_4)_3$ flux. The use of AlF_3 salt in the synthesis reduces the formation temperature of mullite whiskers to 700 °C and

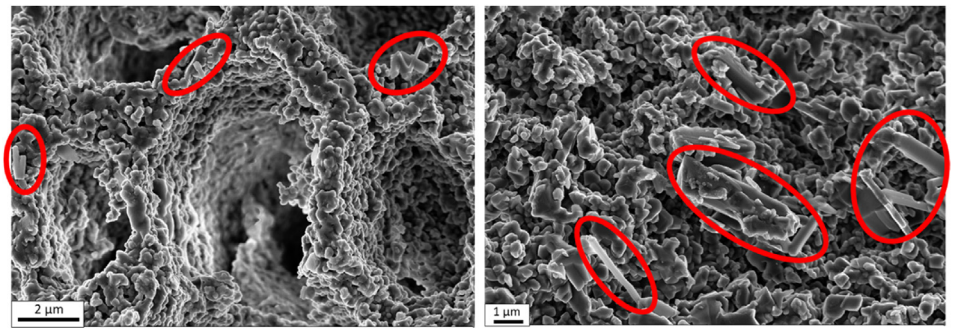

Fig. 8. SEM images of the pore walls (struts) of MA20 monolith, where mullite whiskers act as bridges between alumina particles.

suppresses the formation of the corundum α-Al_2O_3 phase at 1000 °C. The length and aspect ratio of the mullite whiskers are also increased with increasing the amount of AlF_3 salt in the synthesis precursors. The obtained mullite whiskers are applied to fabricate porous alumina-mullite monoliths, which can be used in various potential applications. TBA-based freeze cast samples presented competitive compressive strength while having high porosity. The results show that mullite whiskers can be used as reinforcing material for porous ceramics, metals and composites as a membrane for different filtration processes.

Declaration of competing interest

The authors declare that they have no known competing financial interests or personal relationships that could have appeared to influence the work reported in this paper.

Acknowledgment

We would like to thank Prof. Dr. Dietmar Stephan and Mr. David Dahncke from Chair of Building Materials and Construction Chemistry, TU Berlin, for performing the MIP measurements. A. Abdullayev expresses his gratitude to the German Academic Exchange Service (DAAD) for scholarship support (grant number 91611173). We acknowledge support by the German Research Foundation and the Open Access Publication Fund of TU Berlin.

References

[1] Mullite, H. Schneider, in: S. Komarneni (Ed.), Wiley-VCH Verlag GmbH & Co. KGaA, Weinheim, 2005, ISBN 9783527607358.
[2] A. Abdullayev, M.F. Bekheet, D.A.H. Hanaor, A. Gurlo, Materials and applications for low-cost ceramic membranes, Membranes 9 (2019), https://doi.org/10.3390/membranes9090105.
[3] S. Komarneni, H. Schneider, K. Okada, Mullite synthesis and processing, in: Mullite, H. Schneider, S. Komarneni (Eds.), Wiley-VCH Verlag GmbH & Co. KGaA, Weinheim, 2005, ISBN 9783527607358, pp. 251–348.
[4] P. Zhang, J. Liu, H. DU, Z. Li, S. Li, S. Li, R. Xu, Molten salt synthesis of mullite whiskers from various alumina precursors, J. Alloys Compd. 491 (2010) 447–451, https://doi.org/10.1016/j.jallcom.2009.10.220.
[5] R. El Ouatib, S. Guillemet-Fritsch, B. Durand, A. Samdi, L. Er-Rakho, R. Moussa, Reactivity of aluminum sulfate and silica in molten alkali-metal sulfates in order to prepare mullite, J. Eur. Ceram. Soc. 25 (2005) 73–80, https://doi.org/10.1016/j.jeurceramsoc.2003.12.002.
[6] S. Hashimoto, A. Yamaguchi, Synthesis of α–Al2O3 platelets using sodium sulfate flux, J. Mater. Res. 14 (1999) 4667–4672, https://doi.org/10.1557/JMR.1999.0631.
[7] T. Kimura, Molten salt synthesis of ceramic powders. In Optimization of Ceramics Grinding, in: E.C. Bianchi, A.E. Diniz, P.R.d. Aguiar, R.C. Canarim (Eds.), INTECH Open Access Publisher, 2011, ISBN 978-953-307-505-1.
[8] X. Liu, N. Fechler, M. Antonietti, Salt melt synthesis of ceramics, semiconductors and carbon nanostructures, Chem. Soc. Rev. 42 (2013) 8237–8265, https://doi.org/10.1039/c3cs60159e.
[9] S. Hashimoto, A. Yamaguchi, Synthesis of needlelike mullite particles using potassium sulfate flux, J. Eur. Ceram. Soc. 20 (2000) 397–402, https://doi.org/10.1016/S0955-2219(99)00180-6.
[10] P. Zhang, J. Liu, H. DU, Z. Li, S. Li, C. Chen, Influence of silica sources on morphology of mullite whiskers in Na2SO4 flux, J. Alloys Compd. 484 (2009) 580–584, https://doi.org/10.1016/j.jallcom.2009.04.138.
[11] T. Yang, P. Qiu, M. Zhang, K.-C. Chou, X. Hou, B. Yan, Molten salt synthesis of mullite nanowhiskers using different silica sources, International Journal of Minerals, Metallurgy, and Materials 22 (2015) 884–891, https://doi.org/10.1007/s12613-015-1146-3.
[12] Xuedong Li, Boquan Zhu, Shaowei Zhang, The effects of molten salts on the formation of mullite whiskers, Available online, http://en.cnki.com.cn/Article_en/CJFDTotal-COSE2008S1078.htm. (Accessed 27 November 2019).
[13] Boquan Zhu, Hao Rui, Xuedong Li, Effects of synthesizing temperature on formation of mullite whiskers in molten sodium sulfate medium, Available online, http://en.cnki.com.cn/Article_en/CJFDTotal-COSE2009S2002.htm. (Accessed 27 November 2019).
[14] P. Zhang, J. Liu, H. DU, S. Li, R. Xu, A facile preparation of mullite Al2(Al(2.8)Si(1.2))O(9.6) nanowires by B2O3-doped molten salts synthesis, Chem. Commun. 46 (2010) 3988–3990, https://doi.org/10.1039/b927556h.
[15] A. Kool, P. Thakur, B. Bagchi, N.A. Hoque, S. Banerjee, S. Das, Salt-melt synthesis of B2O3 , P2O5 and V2O5 modified high-alumina mullite nanocomposites with promising photoluminescence properties, Mater. Res. Express 4 (2017) 105005, https://doi.org/10.1088/2053-1591/aa8c34.
[16] K. Okada, N. Otuska, Synthesis of mullite whiskers and their application in composites, J. Am. Ceram. Soc. 74 (1991) 2414–2418, https://doi.org/10.1111/j.1151-2916.1991.tb06778.x.
[17] A. Abdullayev, F. Zemke, A. Gurlo, M.F. Bekheet, Low-temperature fluoride-assisted synthesis of mullite whiskers, RSC Adv. 10 (2020) 31180–31186, https://doi.org/10.1039/D0RA05997H.
[18] H.Y. Chang, T.F. Lee, T. Ejima, Effect of alkali-metal oxide and fluoride on mold flux viscosity, ISIJ Int. 27 (1987) 797–804, https://doi.org/10.2355/isijinternational1966.27.797.
[19] E. Milke, B. Friedrich, A. Sydykov, A. Arnold, Solubility of CaF2 in NaCl-KCl salt flux for Al-recycling and its effect on Al-loss, Proceedings of EMC (2005) 1537–1548.
[20] H. Schneider, Mullite Fibers, in: Mullite, H. Schneider, S. Komarneni (Eds.), Wiley-VCH Verlag GmbH & Co. KGaA, Weinheim, 2005, ISBN 9783527607358, pp. 377–396.
[21] S. Canumalla, S.A. Dynan, D.J. Green, R.B. Bhagat, R.N. Pangborn, Mechanical behavior of mullite fiber reinforced aluminum alloy composites, J. Compos. Mater. 29 (1995) 653–670, https://doi.org/10.1177/002199839502900506.
[22] F. Han, Z. Zhong, Y. Yang, W. Wei, F. Zhang, W. Xing, Y. Fan, High gas permeability of SiC porous ceramics reinforced by mullite fibers, J. Eur. Ceram. Soc. 36 (2016) 3909–3917, https://doi.org/10.1016/j.jeurceramsoc.2016.06.048.
[23] C. Kaya, E. Butler, A. Selcuk, A. Boccaccini, M. Lewis, Mullite (Nextel™ 720) fibre-reinforced mullite matrix composites exhibiting favourable thermomechanical properties, J. Eur. Ceram. Soc. 22 (2002) 2333–2342, https://doi.org/10.1016/S0955-2219(01)00531-3.
[24] C. Li, C. Bian, Y. Han, C.-A. Wang, L. An, Mullite whisker reinforced porous anorthite ceramics with low thermal conductivity and high strength, J. Eur. Ceram. Soc. 36 (2016) 761–765, https://doi.org/10.1016/j.jeurceramsoc.2015.10.002.
[25] H. Zhang, Y. Zhang, B. Wang, J. Yang, Preparation and characterization of continuous alumina based fiber reinforced with orientated mullite whisker, Chem. Eng. J. 268 (2015) 109–115, https://doi.org/10.1016/j.cej.2014.12.101.
[26] T. Robertson, X. Huang, R. Kearsey, High temperature performance of mullite whisker-reinforced ZTA, J. Compos. Mater. 50 (2016) 3719–3729, https://doi.org/10.1177/0021998315624498.
[27] D. Schneider, S. Wassersleben, M. Weiß, R. Denecke, A. Stark, D. Enke, A generalized procedure for the production of high-grade, porous biogenic silica, Waste Biomass Valor 11 (2020) 1–15, https://doi.org/10.1007/s12649-018-0415-6.
[28] A. Bahrami, U. Simon, N. Soltani, S. Zavareh, J. Schmidt, M.I. Pech-Canul, A. Gurlo, Eco-fabrication of hierarchical porous silica monoliths by ice-templating of rice husk ash, Green Chem. 19 (2017) 188–195, https://doi.org/10.1039/C6GC02153K.
[29] S. Zavareh, A. Hilger, K. Hirselandt, O. Goerke, I. Manke, J. Banhart, A. Gurlo, Fabrication of cellular and lamellar $LiFePO_4$/C Cathodes for Li-ion batteries by unidirectional freeze-casting method, J. Ceram. Soc. Japan 124 (2016) 1067–1071, https://doi.org/10.2109/jcersj2.16126.
[30] Rodriguez-Carvajal, J. Fullprof, A program for Rietveld refinement and pattern matching analysis, Satellite meeting on powder diffraction of the XV congress of the IUCr (1990) 127.

[31] L.W. Finger, D.E. Cox, A.P. Jephcoat, A correction for powder diffraction peak asymmetry due to axial divergence, J. Appl. Crystallogr. 27 (1994) 892–900, https://doi.org/10.1107/S0021889894004218.
[32] C.A. Schneider, W.S. Rasband, K.W. Eliceiri, NIH Image to ImageJ: 25 years of image analysis, Nat. Methods 9 (2012) 671–675, https://doi.org/10.1038/nmeth.2089.
[33] C21 Committee, Test Methods for Determination of Water Absorption and Associated Properties by Vacuum Method for Pressed Ceramic Tiles and Glass Tiles and Boil Method for Extruded Ceramic Tiles and Non-tile Fired Ceramic Whiteware Products, ASTM International, West Conshohocken, PA, 2018.
[34] T. Ban, K. Okada, Structure refinement of mullite by the Rietveld method and a new method for estimation of chemical composition, J. Am. Ceram. Soc. 75 (1992) 227–230, https://doi.org/10.1111/j.1151-2916.1992.tb05473.x.
[35] J.A. Pask, H. Schneider, Phase equilibria and stability of mullite, in: Mullite, H. Schneider, S. Komarneni (Eds.), Wiley-VCH Verlag GmbH & Co. KGaA, Weinheim, 2005, ISBN 9783527607358, pp. 227–249.
[36] R.R. Monteiro, A. Sabioni, Preparation of mullite whiskers derived from topaz doped with rare earth oxides for applications in composite materials, Ceram. Int. 42 (2016) 49–55, https://doi.org/10.1016/j.ceramint.2015.08.147.
[37] P. Peng, C. Sorrell, Preparation of mullite whiskers from topaz decomposition, Mater. Lett. 58 (2004) 1288–1291, https://doi.org/10.1016/j.matlet.2003.09.046.
[38] W. Wang, H. Li, K. Lai, K. Du, Preparation and characterization of mullite whiskers from silica fume by using a low temperature molten salt method, J. Alloys Compd. 510 (2012) 92–96, https://doi.org/10.1016/j.jallcom.2011.08.089.
[39] B.Q. Zhu, X.D. Li, R. Hao, H.Z. Wang, Preparation of mullite powder by aluminum sulfate and silica in molten sodium sulfate, KEM 336–338 (2007) 924–926. https://doi.org/10.4028/www.scientific.net/KEM.336-338.924.
[40] X. Delong, L. Yongqin, J. Ying, Z. Longbao, G. Wenkui, Thermal behavior of aluminum fluoride trihydrate, Thermochim. Acta 352–353 (2000) 47–52, https://doi.org/10.1016/S0040-6031(99)00436-0.
[41] D. Freyer, W. Voigt, K. Köhnke, The phase diagram of the system Na2SO4 - CaSO4, Eur. J. Solid State Inorg. Chem. 35 (1998) 595–606, https://doi.org/10.1016/S0992-4361(99)80001-0.
[42] G.K. Çılgı, H. Cetişli, Thermal decomposition kinetics of aluminum sulfate hydrate, J. Therm. Anal. Calorim. 98 (2009) 855–861, https://doi.org/10.1007/s10973-009-0389-5.
[43] E.M. Levin, H.F. McMurdie, Phase Diagrams for Ceramists, 1975, 1975 supplement.
[44] B.O. Mysen, D. Virgo, Interaction between fluorine and silica in quenched melts on the joins SiO2-AlF3 and SiO2-NaF determined by Raman spectroscopy, Phys. Chem. Miner. 12 (1985) 77–85, https://doi.org/10.1007/BF01046830.
[45] Y.P. Zaykov, A.V. Isakov, I.D. Zakiryanova, O.G. Reznitskikh, O.V. Chemezov, A.A. Redkin, Interaction between SiO2 and a KF-KCl-K2SiF6 melt, J. Phys. Chem. B 118 (2014) 1584–1588, https://doi.org/10.1021/jp4086816.
[46] T. Yang, J. Chen, L. Li, K.-C. Chou, X. Hou, Template free synthesis of highly ordered mullite nanowhiskers with exceptional photoluminescence, Ceram. Int. 41 (2015) 9560–9566, https://doi.org/10.1016/j.ceramint.2015.04.016.
[47] K.L. Scotti, D.C. Dunand, Freeze casting – a review of processing, microstructure and properties via the open data repository, FreezeCasting.net. *Progress in Materials Science* 94 (2018) 243–305, https://doi.org/10.1016/j.pmatsci.2018.01.001.
[48] T.Y. Yang, H.B. Ji, S.Y. Yoon, B.K. Kim, H.C. Park, Porous mullite composite with controlled pore structure processed using a freeze casting of TBA-based coal fly ash slurries, Resour. Conserv. Recycl. 54 (2010) 816–820, https://doi.org/10.1016/j.resconrec.2009.12.012.
[49] J.H. Lee, H.J. Choi, S.Y. Yoon, B.K. Kim, H.C. Park, Porous mullite ceramics derived from coal fly ash using a freeze-gel casting/polymer sponge technique, J. Porous Mater. 20 (2013) 219–226.
[50] R. Liu, J. Yuan, C.-A. Wang, A novel way to fabricate tubular porous mullite membrane supports by TBA-based freezing casting method, J. Eur. Ceram. Soc. 33 (2013) 3249–3256, https://doi.org/10.1016/j.jeurceramsoc.2013.06.005.
[51] R. Liu, F. Zhang, W. Su, H. Zhao, C.-A. Wang, Impregnation of porous mullite with Na2SO4 phase change material for thermal energy storage, Sol. Energy Mater. Sol. Cell. 134 (2015) 268–274, https://doi.org/10.1016/j.solmat.2014.12.012.
[52] H.J. Choi, T.Y. Yang, S.Y. Yoon, B.K. Kim, H.C. Park, Porous alumina/zirconia layered composites with unidirectional pore channels processed using a tertiary-butyl alcohol-based freeze casting, Mater. Chem. Phys. 133 (2012) 16–20, https://doi.org/10.1016/j.matchemphys.2011.12.055.